THE JOURNAL OF PHYSICAL CHEMISTRY C
A JOURNAL OF THE AMERICAN CHEMICAL SOCIETY

pubs.acs.org/JPCC

Article

Morphological Study of a Self-Organized Corrole Film on a Gold Crystal, both in Solution and after Solvent Evaporation

Massimo Fanfoni, Beatrice Bonanni,* Roberto Martini, Anna Sgarlata, Fabrizio Caroleo, Roberto Paolesse, and Claudio Goletti

Cite This: *J. Phys. Chem. C* 2023, 127, 12702−12707

Read Online

ACCESS | Metrics & More | Article Recommendations

ABSTRACT: The morphology of the film created by the aggregation of corrole molecules from ethanol solution onto the surface of gold substrate was studied by scanning tunneling microscopy both: (i) in situ, namely in quasi-equilibrium (wet sample), and (ii) ex situ, i.e., removing the substrate from the fluid cell and leaving the residual amount of solution on the substrate to desiccate (dry sample). Despite the different conditions, the morphology of the corrole overlayer formed on the film of molecules is reminiscent, in both cases, of the leopard skin; the "speckles" are actually areas where the molecular overlayer of flat molecules is not completed. We quantitatively compared these two similar morphologies by studying the power spectral density of the images, the fractal dimension D_p of the hole perimeters, and the cumulative distribution function of the hole areas. We found that the last layer of both films, in spite of very different formation conditions, differed from each other only by a scale factor.

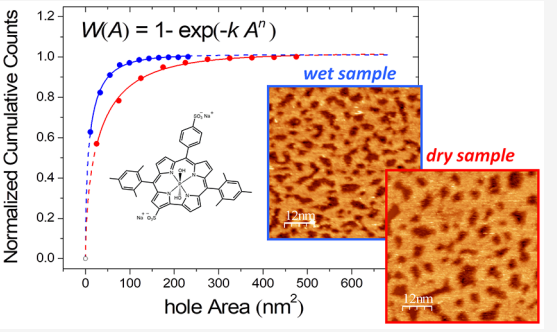

INTRODUCTION

The possibility to realize molecular materials with desired properties by rational synthetic approaches through the developments of organic syntheses and supramolecular chemistry concepts has witnessed an extraordinary boost in recent years, with the definition of several routes for the preparation of molecules tailored with the desired functionalities.[1] The subsequent step for the realization of functional devices is the transfer of the target organic compound from the solution to the solid surface of the final device. While the synthetic route and the characterization of the molecule have been well rationalized, the subsequent step for the formation of the molecular layer is far less developed, although several techniques have been proposed for the formation of the organic thin layers.[2−4] While the definition of the different factors that influence the molecular packing in the formation of the solid layer is self-rewarding from a theoretical point of view, it can also offer useful hints for the control of the film morphology, a key step for the realization of a reliable device.

In the present work, we want to investigate with a certain detail some interesting similarities and dissimilarities in the morphologies that corrole films display when they are grown in quite different environments (dry or wet).

We previously studied the morphology to which the solution of corrole molecules in ethanol gives rise, when placed in contact with the Au(111) surface.[5] The experiments were performed for two concentrations of the dihydroxy phosphorus (V) [10-(4-sulfonatophenyl)-5,15-dimesityl-2-sulfonatocorrole] disodium,[6,7] 1.1×10^{-7} and 5.5×10^{-5} mol/L, and the film was characterized in fluid ambient. Here, the sample obtained from the lower concentration is of our interest and, from now on, it will be referred as wet. The latter, displayed a surface morphology with an extremely variegated landscape; but, among others, there were areas where the morphology was characterized by small holes of different shape and size (leopard skin look). Such morphology, which pertains to the last molecular layer, is obtained after a long immersion time of the gold crystal substrate in the solution, when variations are insignificant.[5] In a second part of that experiment, the gold sample was then removed from the fluid cell and the residual amount of solution on the substrate was let dry in air (from now on referred as dry sample). As in the wet case, the overlayer is formed on top of an already existing film of molecules. Even in the dry case, the morphology resembles that of a leopard skin. The main difference which, at first glance (see Figure 2 ahead), distinguishes the leopard skin of the dry sample from that of the wet one is the size of the holes and their spacing, but nothing can be said about their size distribution and whether we can deduce from this any indication that justifies their alikeness and/or

Received: February 24, 2023
Revised: June 8, 2023
Published: June 22, 2023

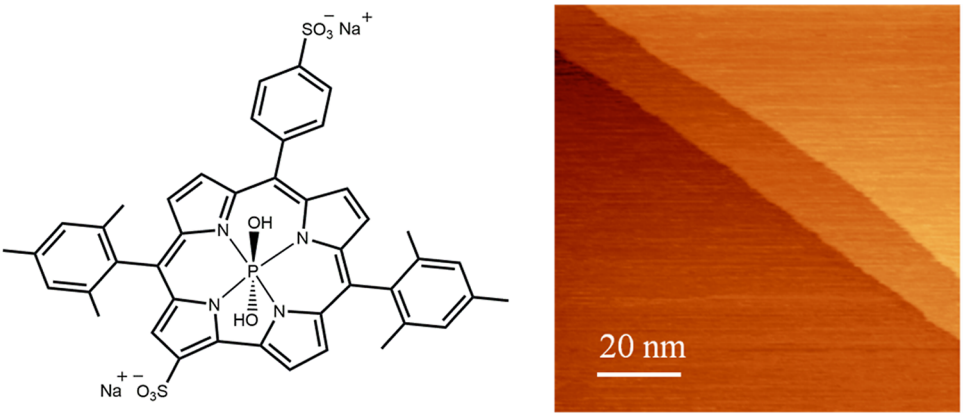

Figure 1. Schematic representation of dihydroxy phosphorus (V) [10-(4-sulfonatophenyl)-5,15-dimesityl-2-sulfonatocorrole] disodium and typical STM image showing terraces of the clean gold surface in air; V_{bias} = −300 mV, I_{tunn} = 1 nA.

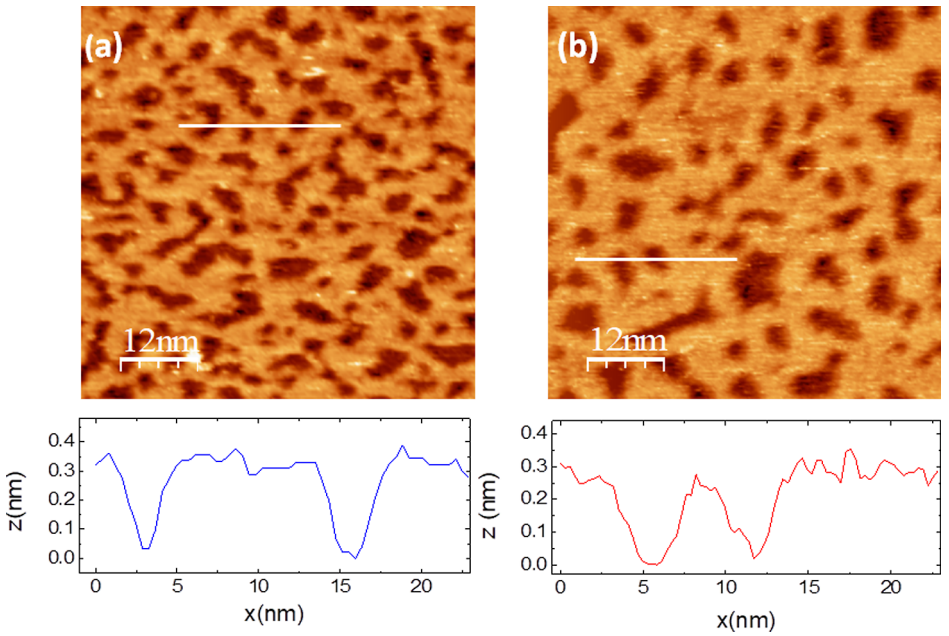

Figure 2. Representative STM images of the corrole film on the Au(111) substrate for the wet (a) and the dry (b) samples. The STM images were recorded in the corrole/ethanol solution 1.1 × 10^{-7} mol/L for the wet sample and in air for the dry sample, with V_{bias} = − 300 mV and I_{tunn}^{wet} = 0.1 nA, I_{tunn}^{dry} = 0.02 nA. Line profiles indicate hole depth corresponding to the thickness of one or two flat corroles.

dissimilarity. To make a quantitative comparison between the two overlayers, we made use of three quantities that translate the morphology into numbers: the characteristic hole distance (d_{char}) returned by the power spectral density (PSD) of the STM image, the fractal dimension D_P of the hole perimeters, and the cumulative distribution function (CDF) of the hole areas.

MATERIALS AND METHODS

Dihydroxy phosphorus (V) [10-(4-sulfonatophenyl)-5,15-dimesityl-2-sulfonatocorrole] disodium was synthesized following the methods mentioned in the literature.[6] The schematic representation of the molecule is shown in Figure 1.

The Au(111) single crystal (MaTeck GmbH, Germany) was cleaned by flame-annealing and the clean surface (Figure 1) was characterized as described elsewhere.[5] Ethanol solutions of this corrole with a concentration C = 1.1 × 10^{-7} mol/L, well below the solubility limit, were prepared; UV−vis spectra of the solution confirmed the absence of macrocycle aggregation.

For the wet sample, STM measurements were performed in 2.5 mL of ethanol/corrole solution by a home-made electrochemical scanning tunneling microscope (EC-STM);[8,9] tungsten tips were electrochemically etched and coated (except the apex) with glue to reduce, far below the tunneling current level, any faradic current flowing through the tip. Images showing the leopard skin morphology were recorded well after the early phases of film formation,[5] when an asymptotic morphology was achieved (about 120 min).

The dry sample was obtained by removing the specimen from the fluid cell after the in situ measurements and letting the residual amount of solution (70 μL) dry overnight; the following STM images were recorded in air.

All the quoted bias voltages V_{bias} refer to the tip (images acquired with negative bias correspond to tunneling into empty states of the sample).

STM images were analyzed by WSxM,[10] ImageJ,[11] and MATLAB[12] software. The latter was also used for numerical simulations.

https://doi.org/10.1021/acs.jpcc.3c01286
J. Phys. Chem. C 2023, 127, 12702−12707

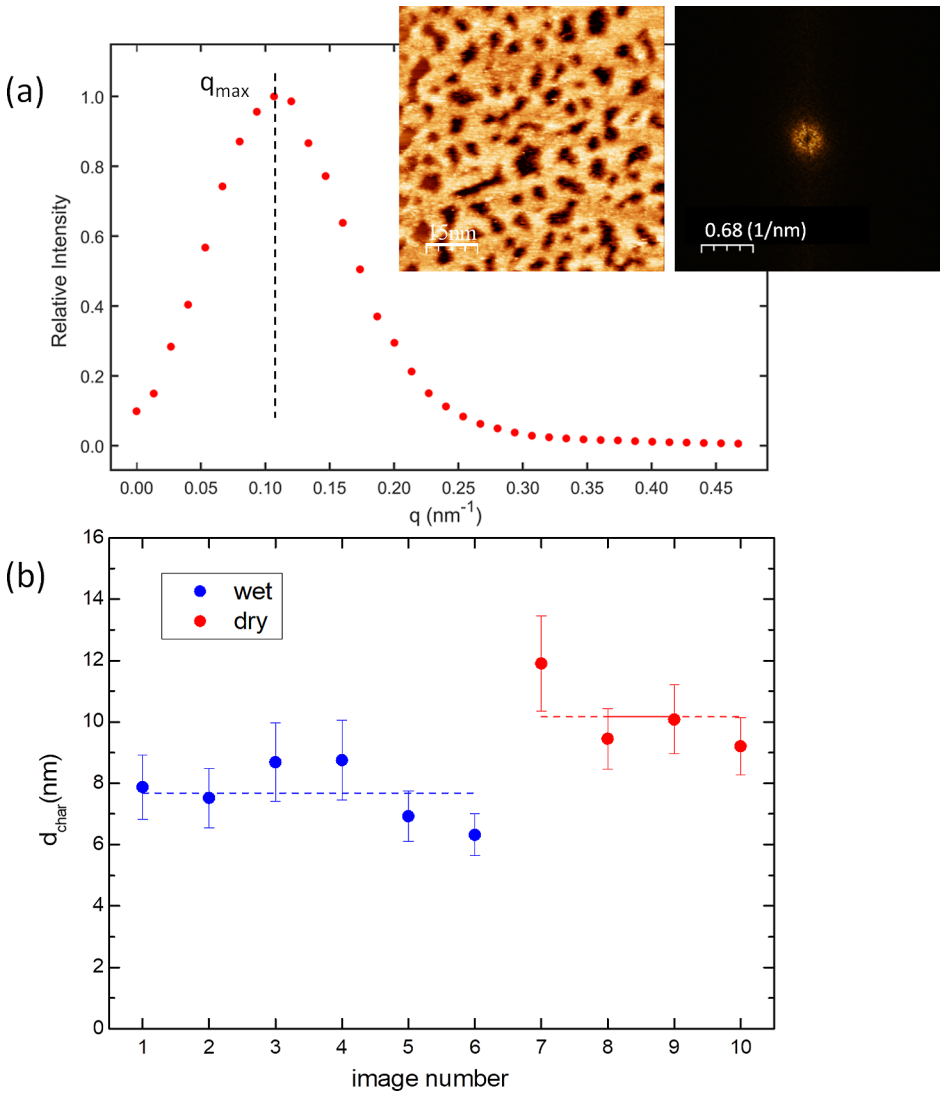

Figure 3. (a) PSD and q_{max} of the 2D-FFT analysis (inset) of a representative STM image for the dry sample. $V_{bias} = -300$ mV, $I_{tunn}^{dry} = 0.02$ nA. (b) Values of characteristic average hole spacing d_{char} obtained from the q_{max} values of several STM images for the wet (blue) and the dry (red) samples. Dashed lines correspond to the average values.

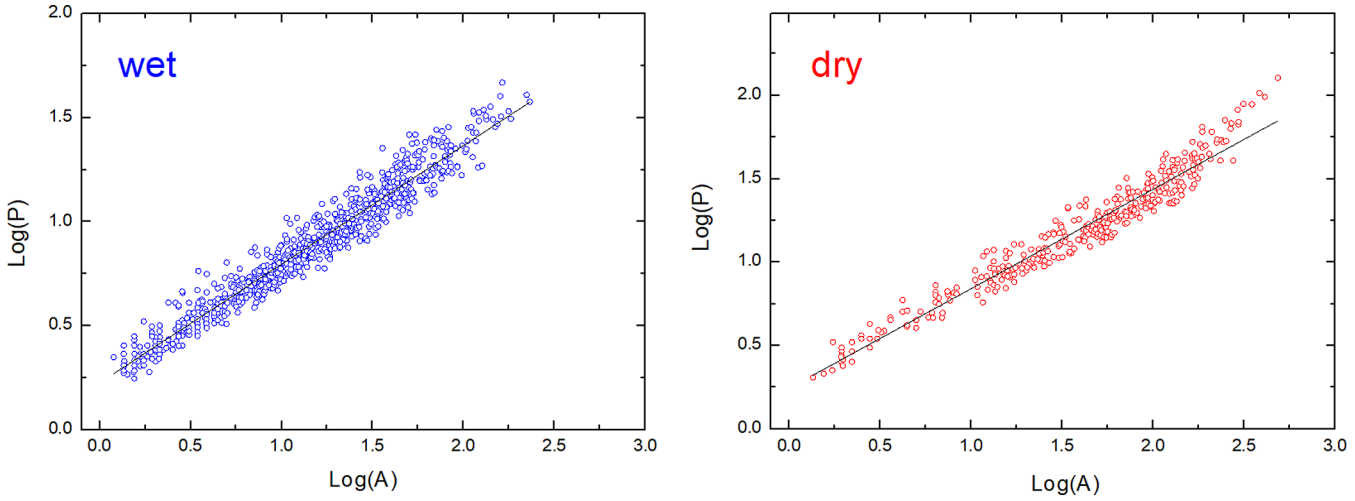

Figure 4. Plot of log P vs log A for the holes in the corrole overlayer of the wet (left panel, blue) and the dry (right panel, red) samples, as observed in several STM images (see for instance Figure 2). Open symbols correspond to experimental values of P and A of about 830 and 410 different holes from several STM images of the wet and the dry samples, respectively. Best linear fit, represented with continuous line, provides the slope $\sigma = D_p/2$.

https://doi.org/10.1021/acs.jpcc.3c01286
J. Phys. Chem. C 2023, 127, 12702−12707

RESULTS AND DISCUSSION

Figure 2a,b show typical STM images of, respectively, the wet and dry samples displaying the leopard skin morphology. The molecular overlayer, whose thickness corresponds to one or two flat corroles molecules (see line profiles in Figure 2), forms on top of an already existing film of molecules;[5] the analysis of leopard skin STM images provides the fraction of surface area covered by the holes, namely $\Theta^{wet} = 0.32 \pm 0.02$ and $\Theta^{dry} = 0.32 \pm 0.05$.

The characteristic average hole spacing d_{char} is a key parameter for a quantitative description of the morphology and can be estimated using the two-dimensional fast Fourier transform (2D FFT) of the STM images. For example, in Figure 3a (inset), we show a representative STM topography of the dry sample together with its 2D FFT; the radially averaged power spectrum provides the intensity vs momentum q correlation plot (PSD). The spatial correlation is characterized by a well-defined peak of the PSD at q_{max}, which returns the in-plane characteristic distance d_{char} among holes in the overlayer. Similar analysis on several images for the wet and the dry samples returned the characteristic distances reported in Figure 3b. The average values are different within the error: $\langle d_{char}^{dry} \rangle = (10.2 \pm 0.6)$ nm, $\langle d_{char}^{wet} \rangle = (7.7 \pm 0.4)$ nm; the holes for the dry case are further apart.

Remaining in the sphere of the geometrical characterization of the two morphologies, we determined the fractal dimension D_p of the hole rims by studying the perimeter (P) vs area (A) relation, which is described by the following power law[13,14]

$$P \propto A^{\sigma} \tag{1}$$

where, according to Mandelbrot,[15] the scaling exponent is $\sigma = D_P/D_A$, with D_A the fractal dimension of the area; however, D_A reduces to 2 for a compact image plane[16] so that the scaling exponent is $\sigma = D_P/2$. The log P vs log A[13] plot for both the wet and the dry samples is reported in Figure 4. The resulting linear behavior covers more than two decades of the area axes; the linear regression best fit analysis to the data returns for the perimeter fractal dimension the values $D_P^{wet} = 1.14 \pm 0.03$ and $D_P^{dry} = 1.19 \pm 0.02$, which are equal within the statistical error (3σ), proving the geometrical similarity of the hole shape in the wet and the dry cases.

The third quantity we studied in order to characterize the films is the cumulative size distribution of the holes, in particular the normalized cumulative distribution of their areas. The behavior is displayed in Figure 5, and we found that the experimental data fit the Weibull function[17] very well

$$W(x) = 1 - e^{-kx^n} \tag{2}$$

which is the curve passing through the experimental points in the figure, here x indicates the hole area expressed in square nanometers.

The most significant fit parameter n, called shape parameter, is the same within a single standard deviation both for the dry and wet samples: $n^{wet} = 0.55 \pm 0.02$ and $n^{dry} = 0.59 \pm 0.03$. The expected value of a stochastic variable that follows the Weibull distribution (eq 2) is given as follows:

$$E[X] = \frac{\nu}{k^{\nu}}\Gamma(\nu) \tag{3}$$

where $\Gamma(\nu)$ is the Euler gamma function and $\nu = \frac{1}{n}$. The calculation from the fit parameters provides, for the expected hole areas, the values $E^{wet}[A] \cong 20$ nm^2 and $E^{dry}[A] \cong 54$ nm^2.

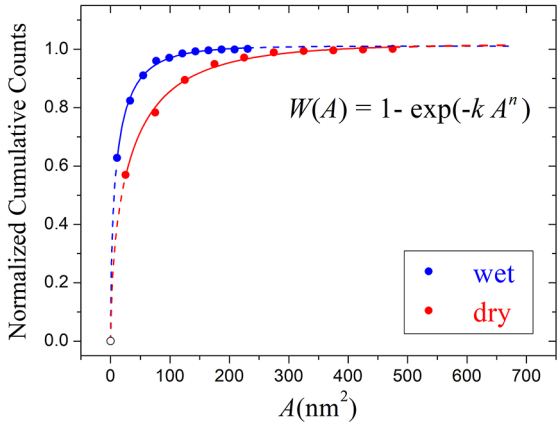

Figure 5. Symbols represent experimental hole area cumulative counts for both the wet (blue) and the dry (red) samples normalized to unity. Experimental data have been obtained from several STM images by measuring the area of hundreds of holes. The points fit the Weibull distribution (continuous line) written in the frame (eq 2); the best fit parameters are: $n^{wet} = 0.55 \pm 0.02$, $k^{wet} = 0.258 \pm 0.014$, adjusted R-squared = 0.997 and $n^{dry} = 0.59 \pm 0.03$, $k^{dry} = 0.119 \pm 0.012$, and adjusted R-squared = 0.995. The first part of Weibull curve is dashed since the theoretical point (0,0) is not included in the fitting process.

These results not only confirm what we have already stated based on a simple visual inspection (namely, that the hole size of the dry sample is greater than that of the wet sample) but, more importantly, quantify the difference in about a factor 3 for the area size. As far as the differences in the characteristic hole distance and average areas are concerned, we believe that they are due to a swelling effect of ethanol in solution: like a sponge, when the solvent evaporates, the film shrinking induces the increase of the hole size. Such phenomenon, in turn, gives rise to the merging among neighboring holes with the consequent increase of the average hole−hole distance.

The Weibull distribution has a lot of applications in many different fields of science and technology,[18−25] in particular, among others, it has been profitably employed to describe the size of particles obtained in fragmentation processes (e.g., grinding, milling, and crushing operations).[26−30] It goes without saying that our size distribution has to do with a kind of "particles" of completely different nature: they are holes, namely lack of molecules. This simple fact is already interesting in itself, and we wondered if we were dealing with something more general. For this reason, we tried to test numerically whether the Weibull distribution could be, at least under certain hypothesis, universal.

Therefore, we wrote a code in MATLAB[12] for simulating the growth of clusters, where disks of equal radius r are generated at random on a 2000 × 2000 square lattice, until an assigned coverage Θ is reached; the 2D morphology results in clusters (holes) each composed by a certain number of overlapped disks. Figure 6a shows an example corresponding to the coverage $\Theta = 0.35$. Notably, the cumulative area distribution of the simulated clusters well fits the Weibull eq 2 (adjusted R-squared = 0.9992). As the simulation disks are generated with an increasing degree of spatial correlation, for instance introducing the constraint that does not allow the disk centers to lay closer than a given distance R_C (correlation radius) from each other, cluster areas gradually deviate from the distribution of eq 2. This effect is evidenced in the example reported in Figure 6b, where the points are generated by introducing a spatial correlation with $R_C = 75$ and

https://doi.org/10.1021/acs.jpcc.3c01286
J. Phys. Chem. C 2023, 127, 12702−12707

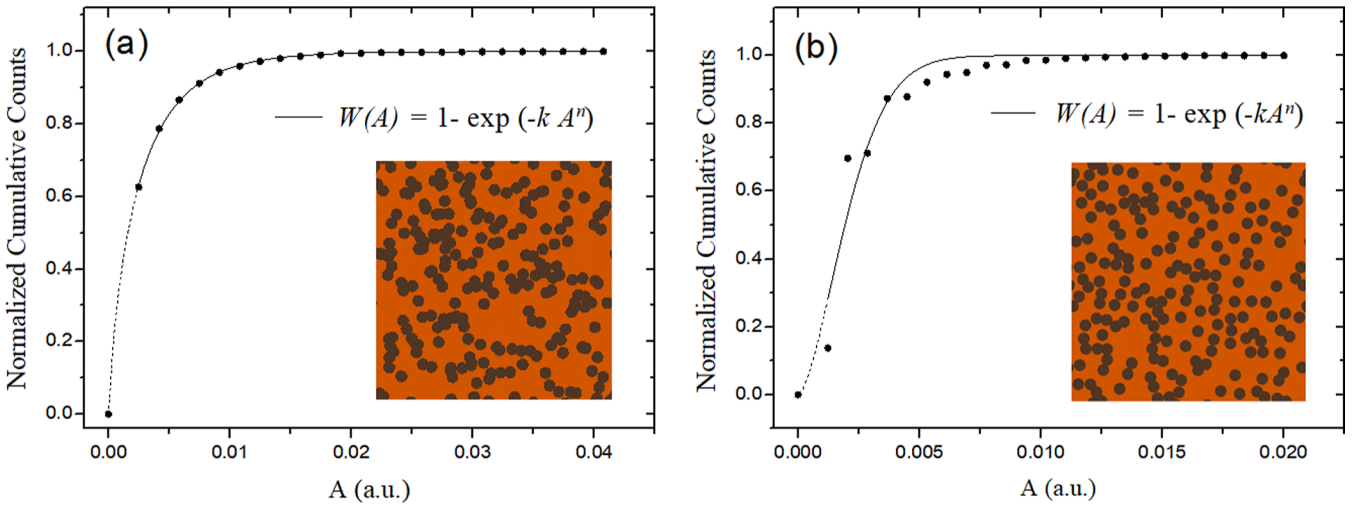

Figure 6. Symbols represent normalized cumulative counts of cluster areas obtained by averaging over 50 simulations for disks of radius r = 50 pixels, on a 2000 × 2000 pixels lattice. Disks are generated: (a) at random, (b) with spatial correlation as described in the text. Each simulation is stopped at coverage Θ = 0.35. The fits to the Weibull distribution (continuous line) return the adjusted R-squared 0.9992 and 0.9203, respectively. First part of Weibull curve is dashed since the theoretical point (0,0) is not included in the fitting process. Insets: examples of simulated images after a single iteration.

the continuous line is the curve fit (adjusted R-squared = 0.9203).

We emphasize that our simulations are only meant to test how general the Weibull distribution is, once a spatial distribution of clusters is given; we do not intend to reproduce exactly the morphology of the film.

Summing up.

(i) for both wet and dry samples, the cumulative size distribution of holes fit the Weibull distribution (eq 2); in a sense, it is as if the carpet of molecules were to undergo a tearing process that from the statistical point of view is equivalent to a process of grinding, for instance, of rocks.

(ii) the simulations show that clusters obtained from randomly generated disks, have areas that distribute according to the Weibull function (eq 2);

(iii) if the simulation disks are generated with a spatial correlation, the Weibull distribution of eq 2 does not describe clusters' areas distribution satisfactorily.

On the basis of the previous points, we conjecture that hole formation may occur according to the following process: initially small holes, a few molecules wide, are formed randomly over the entire surface and then grow and overlap to form larger holes whose centers of gravity are clearly spatially correlated.

On the other hand, the initial formation of the holes may be traced back to the film instability with respect to the thickness fluctuations.[31−34]

CONCLUSIONS

A solution of corrole molecules in ethanol 1.1×10^{-7} mol/L was made to interact with the Au(111) surface, and the subsequent molecular film formation was analyzed. In particular, the corrole film was formed using two methods: in a liquid environment (wet) and by drying a drop of solution on a pre-existing film of molecules (dry). In both cases, the overlayer evidences the presence of holes, at most two flat molecules deep, randomly distributed over the surface. Despite the different deposition conditions, the last layer morphology of the two films result to differ only for a scale factor. There are two parameters that show that the process of the film formation is independent of the ambient conditions: the fractal dimension D_p of the rims and the exponent n of the Weibull function. The latter excellently describes the distribution of hole sizes and allows to determine that the dry and wet mean hole areas differ of about a factor of 3.

The hole formation in solution, which according to Vrij could take place because of instabilities with respect to thickness fluctuations, is too fast with respect to the typical time scale of the STM image acquisition, and it is impossible to directly monitor and/or study it. However, on the basis of the experimental and simulation results, we have advanced a hypothesis to explain how the morphology of the film evolves until it reaches the final look.

Besides, it is worth pointing out that our choice of the PSD, D_p, and CDF quantities was winning, since they were proven to be excellent for describing the morphology of molecular films.

AUTHOR INFORMATION

Corresponding Author

Beatrice Bonanni − *Department of Physics, Università degli Studi di Roma "Tor Vergata", I-00133 Rome, Italy;* orcid.org/0000-0002-0925-6200; Email: beatrice.bonanni@roma2.infn.it

Authors

Massimo Fanfoni − *Department of Physics, Università degli Studi di Roma "Tor Vergata", I-00133 Rome, Italy*

Roberto Martini − *Department of Physics and Department of Chemical Science and Technologies, Università degli Studi di Roma "Tor Vergata", I-00133 Rome, Italy*

Anna Sgarlata − *Department of Physics, Università degli Studi di Roma "Tor Vergata", I-00133 Rome, Italy*

Fabrizio Caroleo − *Department of Chemical Science and Technologies, Università degli Studi di Roma "Tor Vergata", I-00133 Rome, Italy*

Roberto Paolesse − *Department of Chemical Science and Technologies, Università degli Studi di Roma "Tor Vergata", I-00133 Rome, Italy;* orcid.org/0000-0002-2380-1404

https://doi.org/10.1021/acs.jpcc.3c01286
J. Phys. Chem. C 2023, 127, 12702−12707

Claudio Goletti − *Department of Physics, Università degli Studi di Roma "Tor Vergata", I-00133 Rome, Italy;* orcid.org/0000-0002-4120-6107

Complete contact information is available at: https://pubs.acs.org/10.1021/acs.jpcc.3c01286

Notes

The authors declare no competing financial interest.

■ ACKNOWLEDGMENTS

A.S. and B.B. thank the University of Rome Tor Vergata for funding (Project "GREEN—Growth of coRrole layErs: from propErty tuning to applicatioNs" Progetti di Ateneo Università degli Studi di Roma "Tor Vergata", CUP E83C22000350005). A.S. thanks the Regione Lazio POR FESR Lazio 2014-2020 for funding (Project id 1076780300-0327). Proposal code (POR A0375E0102) "High—electron mobility 2D polymers" (P2DAME, HEM-2DP).

■ REFERENCES

(1) *Molecular Materials: Preparation, Characterization, and Applications*; Malhotra, S., Prasad, B. L. V., Fraxedas, J., Eds.; CRC Press: Boca Raton (USA), 2017, ISBN 9781032339696.

(2) Meng, X. An overview of molecular layer deposition for organic and organic−inorganic hybrid materials: mechanisms, growth characteristics, and promising application. *J. Mater. Chem. A* **2017**, *5*, 18326−18378.

(3) Sassella, A.; Campione, M.; Raimondo, L.; Borghesi, A.; Bussetti, G.; Cirilli, S.; Violante, A.; Goletti, C.; Chiaradia, P. Pseudomorphic growth of organic semiconductor thin films driven by incommensurate epitaxy. *Appl. Phys. Lett.* **2009**, *94*, 073307.

(4) Calloni, A.; Jagadeesh, M. S.; Bussetti, G.; Fratesi, G.; Achilli, S.; Picone, A.; Lodesani, A.; Brambilla, A.; Goletti, C.; Ciccacci, F.; et al. Cobalt atoms drive the anchoring of Co-TPP molecules to the oxygen-passivated Fe(0 0 1) surface. *Appl. Surf. Sci.* **2020**, *505*, 144213.

(5) Bonanni, B.; Fanfoni, M.; Lacal, M.; Sgarlata, A.; Caroleo, F.; Paolesse, R.; Goletti, C. Growth of Corrole Films from Solution: A Nanometer-Scale Study at the Real Solid−Liquid Interface. *J. Phys. Chem. C* **2021**, *125*, 11540−11547.

(6) Naitana, M.; Nardis, S.; Pomarico, G.; Raggio, M.; Caroleo, F.; Cicero, D.; Lentini, S.; Prodi, L.; Genovese, D.; Mitta, S.; et al. A Highly Emissive Water-Soluble Phosphorus Corrole. *Chem.—Eur. J.* **2017**, *23*, 905−916.

(7) Bonanni, B.; Fazi, L.; Fanfoni, M.; Sgarlata, A.; Caroleo, F.; Pomarico, G.; Galloni, P.; Sabuzi, F.; Persichetti, L.; Paolesse, R.; Goletti, C. Corroles at the real solid−liquid interface: in situ STM investigation of a water-soluble corrole layer deposited onto Au(111). *Chem.—Eur. J.* **2018**, *24*, 17538−17544.

(8) Wilms, M.; Kruft, M.; Bermes, G.; Wandelt, K. A new and sophisticated electrochemical scanning tunneling microscope design for the investigation of potentiodynamic processes. *Rev. Sci. Instrum.* **1999**, *70*, 3641−3650.

(9) Goletti, C.; Bussetti, G.; Violante, A.; Bonanni, B.; DiGiovannantonio, M.; Serrano, G.; Breuer, S.; Gentz, K.; Wandelt, K. Cu(110) Surface in Hydrochloric Acid Solution: Potential Dependent Chloride Adsorption and Surface Restructuring. *J. Phys. Chem. C* **2015**, *119*, 1782−1790.

(10) Horcas, I.; Fernandez, R.; Gomez-Rodriguez, J.; Colchero, J.; Gómez-Herrero, J.; Baro, A. M. WSXM: A software for scanning probe microscopy and a tool for nanotechnology. *Rev. Sci. Instrum.* **2007**, *78*, 013705.

(11) Rueden, C. T.; Schindelin, J.; Hiner, M. C.; De Zonia, B. E.; Walter, A. E.; Arena, E. T.; Eliceiri, K. W. ImageJ2: ImageJ for the next generation of scientific image data. *BMC Bioinf.* **2017**, *18*, 529−554.

(12) *MATLAB R2022b*; The MathWorks, Inc.: Natick, Massachusetts, United States, 2022.

(13) Florio, B. J.; Fawell, P. D.; Small, M. The use of the perimeter-area method to calculate the fractal dimension of aggregates. *Powder Technol.* **2019**, *343*, 551−559.

(14) Bonanni, B.; Fanfoni, M.; Sgarlata, A.; Caroleo, F.; Paolesse, R.; Goletti, C. Perimeter fractal dimension analysis of corrole islands on Au(111) at the solid-water interface. *J. Porphyrins Phthalocyanines* **2020**, *24*, 959−963.

(15) Mandelbrot, B. *The Fractal Geometry of Nature*; Freeman: San Francisco, 1982.

(16) Zhu, W.; Mohammadi, E.; Diao, Y. Quantitative Image Analysis of Fractal-Like Thin Films of Organic Semiconductors. *J. Polym. Sci., Part B: Polym. Phys.* **2019**, *57*, 1622−1634.

(17) Prabhakar, M. D. N.; Xie, M.; Jiang, R. *Weibull Models*; John Wiley & Sons: New York, 2003.

(18) Zachariev, G. A Statistical Theory of the Damage of Materials. *Mod. Mech. Eng.* **2016**, *06*, 129−150.

(19) Sharif, M. N.; Islam, M. N. The Weibull Distribution as a General Model for Forecasting Technological Change. *Technol. Forecast. Soc. Change* **1980**, *18*, 247−256.

(20) Tsuboi, T.; Takami, J.; Okabe, S.; Inami, K.; Aono, K. Weibull Parameter of Oil-immersed Transformer to Evaluate Insulation Reliability on Temporary Overvoltage. *IEEE Trans. Dielectr. Electr. Insul.* **2010**, *17*, 1863−1868.

(21) Wais, P. A review of Weibull functions in wind sector. *Renewable Sustainable Energy Rev.* **2017**, *70*, 1099−1107.

(22) Bhardwaj, S.; Bhardwaj, N.; Kumar, V. The study of reliability of diesel locomotive engine using weibull distribution. *Int. J. Agric. Stat. Sci.* **2019**, *15*, 549−554.

(23) Zhang, B.; Tang, L.; Roemer, M. Probabilistic Weather Forecasting Analysis for Unmanned Aerial Vehicle Path Planning. *J. Guid. Control. Dyn.* **2014**, *37*, 309−312.

(24) Singh, V. P. On application of the Weibull distribution in hydrology. *Water Resour. Manage.* **1987**, *1*, 33−43.

(25) Putkonen, A.; Nioche, A.; Laine, M.; Kuuramo, C.; Oulasvirta, A. Fragmented Visual Attention in Web Browsing: Weibull Analysis of Item Visit Times. *Lecture Notes in Computer Science*; Springer Nature Switzerland, 2023; Vol. *13981*, pp 62−78. Advances in Information Retrieval. ECIR 2023.

(26) Alderliesten, M. Mean Particle Diameters. Part VII. The Rosin-Rammler Size Distribution: Physical and Mathematical Properties and Relationships to Moment-Ratio Defined Mean Particle Diameters. *Part. Part. Syst. Charact.* **2013**, *30*, 244−257.

(27) Fang, Z.; Patterson, B. R.; Turner, M. E. Modeling particle size distributions by the Weibull distribution function. *Mater. Charact.* **1993**, *31*, 177−182.

(28) Brouwers, H. J. H. Packing fraction of particles with a Weibull size Distribution. *Phys. Rev. E* **2016**, *94*, 012905.

(29) Paluszny, A.; Tang, X. H.; Nejati, M.; Zimmerman, R. W. A direct fragmentation method with Weibull function distribution of sizes based on finite- and discrete element simulations. *J. Solids Struct.* **2016**, *80*, 38−51.

(30) Brown, W. K.; Wohletz, K. H. Derivation of the Weibull distribution based on physical principles and its connection to the Rosin−Rammler and lognormal distributions. *J. Appl. Phys.* **1995**, *78*, 2758−2763.

(31) Vrij, A. Possible mechanism for the spontaneous rupture of thin, free liquid films. *Discuss. Faraday Soc.* **1966**, *42*, 23−33.

(32) Gentili, D.; Foschi, G.; Valle, F.; Cavallini, M.; Biscarini, F. Applications of dewetting in micro and nanotechnology. *Chem. Soc. Rev.* **2012**, *41*, 4430−4443. and references therein

(33) Herminghaus, S.; Fery, A.; Schlagowski, S.; Jacobs, K.; Seemann, R.; Gau, H.; Monch, W.; Pompe, T. Liquid microstructures at solid interfaces. *J. Phys.: Condens. Matter* **2000**, *12*, A57−A74. and references therein

(34) Mukherjee, R.; Sharma, A. Instability, self-organization and pattern formation in thin soft films. *Soft Matter* **2015**, *11*, 8717−8740. and references therein